Charge ordering in stoichiometric FeTe: Scanning tunneling microscopy and spectroscopy

Wei Li, Wei-Guo Yin, Lili Wang, Ke He, Xucun Ma, Qi-Kun Xue, and Xi Chen

Phys. Rev. B **93**, 041101 — Published 4 January 2016

DOI: 10.1103/PhysRevB.93.041101

Charge Ordering in Stoichiometric FeTe

Wei Li,[1,2] Wei-Guo Yin,[3,*] Lili Wang,[1,2] Ke He,[1,2] Xucun Ma,[1,2] Qi-Kun Xue,[1,2] and Xi Chen[1,2,†]

[1] *State Key Laboratory of Low-Dimensional Quantum Physics, Department of Physics, Tsinghua University, Beijing 100084, China*
[2] *Collaborative Innovation Center of Quantum Matter, Beijing 100084, China*
[3] *Condensed Matter Physics and Materials Science Department, Brookhaven National Laboratory, Upton, New York 11973, USA*

We use scanning tunneling microscopy and spectroscopy to reveal a unique stripy charge order in a parent phase of iron-based superconductors in stoichiometric FeTe epitaxy films. The charge order has unusually the same—usually half—period as the spin order. We also found highly anisotropic electron band dispersions being large and little along the ferromagnetic (crystallographic b) and antiferromagnetic (a) directions, respectively. Our data suggest that the microscopic mechanism is likely of the Stoner type driven by inter-atomic Coulomb repulsion V_{ij}, and that V_{ij} and charge fluctuations, so far much neglected, be important to the understanding of iron-based superconductors.

PACS numbers: 68.37.Ef, 71.45.Lr, 75.30.Et, 74.70.-b, 81.15.Hi

Strong electronic correlations in numerous transition-metal compounds are usually attributed to intra-atomic Coulomb repulsion U [1]. Strong correlations in multiorbital systems governed by Hunds rule coupling J_H (intra-atomic exchange) was also explored recently [2]. These two mechanisms are identifiable by investigating the broken-symmetry ground states in the parent undoped limit of those materials, where U and $J_{\rm H}$ clearly favour orbital order (OO) and charge order (CO), respectively [3]. However, when the competing impacts of U and $J_{\rm H}$ are comparable, the nature of electronic correlations, a fundamental problem concerning iron-based superconductors (FeSC) [4–13], remains to be elucidated. It is also highly desirable to know if any other interaction would become critical in such an intermediate regime.

Strong correlations in FeSC have been manifested in optical spectroscopy as a substantial reduction in the electrons' kinetic energy [4]. Yet, whether they originate mainly from U or $J_{\rm H}$ is controversial, since the electron motion can be impeded by either type of interactions. In the iron atom or iron oxides, U is usually one order of magnitude larger than $J_{\rm H}$. By contrast, the x-ray experiments suggest that $U \sim 2$ eV and $J_{\rm H} \sim 0.8$ eV in FeSC [5]. This weakening of U but not $J_{\rm H}$ was attributed [20] to the highly polarizable As^{3-}, Se^{2-}, or Te^{2-} anions residing on the low-symmetric crystallographical sites out of the iron planes (Fig. 1A): their electron clouds are ten times easier to be polarized than O^{2-}. Looking into the parent undoped compounds of FeSC, to date, only OO was observed in LaOFeAs, $BaFe_2As_2$, and FeSe [14–17], which seems to support the U mechanism. However, the hypothesis that strong correlations in FeSC are associated with a novel sophisticated $J_{\rm H}$-driven orbital-selective Mott transition, which gives rise to coexisting itinerant and localized electrons, has been of considerable interest [7–13]. Here we report observation of a unique charge order (CO) in stoichiometric FeTe. This evidences that the $J_{\rm H}$ effect is comparable to U in FeSC, indeed. Our further experimental and theoretical analyses suggest that the inter-atomic Coulomb interaction V_{ij} and charge fluctuations [18, 19], so far much neglected, be essential to the understanding of FeSC.

First of all, we stress that the stoichiometry of the samples is critical to our experiments. In this limit such as La_2CuO_4 and $LaMnO_3$, the formation of CO incurs an energy cost proportional to U and is prohibited by large U. Charge doping can introduce mixed valence; CO as a result of rearranging those atoms with different valences is thus free of the U penalty [21, 22]. Hence, only the observation of CO in the stoichiometric limits can rule out the leading role of U. The study of stoichiometric FeTe has been hindered by the fact that single crystal $Fe_{1+x}Te$ samples usually contain a sizeable amount of excessive Fe atoms (Fe_x), which are known to dope electrons and bring substantial extrinsic effects such as transforming the metallic FeTe to a semiconductor [23, 24]. To overcome this undesirable complexity, we used the molecular beam epitaxy (MBE) technology to grow stoichiometric FeTe single-crystalline films and performed *in-situ* scanning scanning tunneling microscopy (STM) and spectroscopy (STS) measurements on their surfaces. It is noteworthy that excess Fe atoms could be picked up by the STM tip on a $Fe_{1+x}Te$ surface, yielding a magnetic tip good for visualizing the ordering pattern of spins instead of charges [25]. Thus, the stoichiometry of FeTe samples is particularly critical to the STM study of charge dynamics in them [26–30]. We have verified the absence of any indications of a magnetic STM tip, as reported in Ref. 25, in our measurements (see Supplementary Note 1 [31]).

The experiments were carried out in a Unisoku UHV ^{3}He STM system equipped with a MBE chamber for *in-situ* film growth. The FeTe (001) film was prepared on the graphitized 6H-SiC (0001) substrate. High-purity Fe (99.995%) and Te (99.9999%) were evaporated from two standard Knudsen cells. The growth was performed in

the Te-rich conditions with a nominal Te/Fe flux ratio of ∼15 to avoid excess Fe in the film, while the substrate temperature was held at 310°C. The growth follows the typical layer-by-layer mode. The as-grown films were directly transferred to STM. A polycrystalline PtIr STM tip was used in the experiments. We studied the samples with the thickness of 15, 20, and 30 unit cells and found similar results. We present here the measurements on the 30-unit-cell sample.

Experimental Results—The film undergoes a structural phase transition at $T_s \sim 65$ K where the lattice constants split into long a_{Te} and short b_{Te} (Figs. 1B,1D). Previous studies [23] on bulk FeTe show a tetragonal to monoclinic (nearly orthorhombic) structural phase transition at similar temperature and a simultaneous development of the E-type antiferromagnetic (AFM) spin order (SO) with the long axis of the Te planar lattice along the AFM direction (Fig. 1B). We thus assign the a-axis as the AFM direction and the b-axis as the ferromagnetic (FM) direction in the film.

Most strikingly, Fig. 1D shows a pattern of stripes formed by the topmost Te atoms along the FM direction. The inset of Fig. 1D shows superlattice peaks at $(\pm\frac{\pi}{a_{Te}},0)$, indicating a new lattice period of $2a_{Te}$, in coincidence with that of the E-type SO. Since with the nonmagnetic tip, our measurements are not sensitive to spin but charge (see Supplemental Note 1 [31]), this stripe pattern is recognized as a CO. The STM images at different temperatures (Fig. 2, A to D) show that the stripe order appears along with the structural/magnetic transition: it is barely visible at 63 K and completely disappears at $T_s \sim 65$ K.

The energy dependence of the stripes at 4.2 K is presented in Fig. 2, E to H, with the STM images of the same location under different bias voltages. The pattern is only visible at low energy within ±30 meV of the Fermi level, which rules out the possibility of surface reconstruction. Inside this energy window, the stripes are static and remain unchanged with different bias voltage. We note that previous neutron scattering studies revealed the existence of strong spin fluctuations in the FeTe system: the long-range E-type AFM order only makes a small and very low-energy contribution to the entire spin dynamics, while the higher energy part is governed by other competing orders such as the 2×2 plaquette SO [32]. The appearance of stripes only at low energy suggests that the CO is tied up with the E-type AFM SO rather than the structure transition.

To relate the stripe pattern of the Te anions with the E-type SO of the Fe cations, we mark in Fig. 1B two adjacent Te atoms "A" and "B": If "A" is bright, then "B" must be dark. The key point is that "A" and "B" differ in the configuration of their neighboring Fe spins: "A" is adjacent to one up and three down Fe spins, while "B" is adjacent to one down and three up spins. Therefore, the contrast displayed by the Te atoms is accountable by

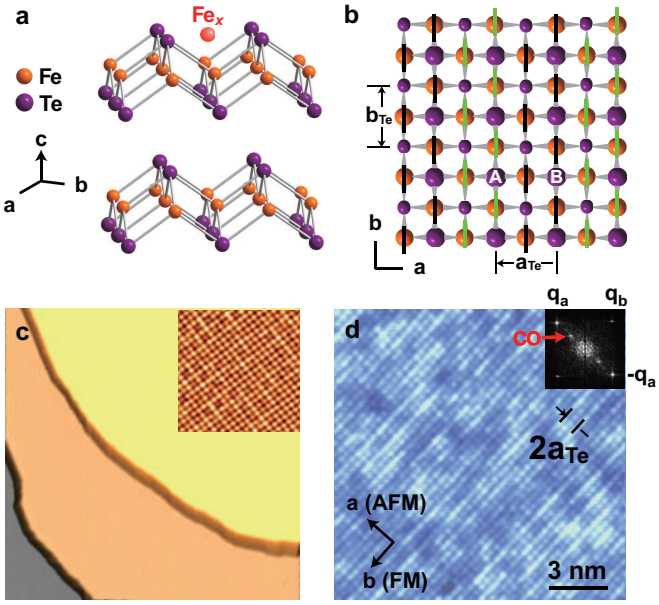

FIG. 1. **Structure and STM topography of Te-terminated FeTe(001) films.** (A) Crystal structure. Excess Fe atoms (Fe_x) if any are located in the Te layer and easily seen by STM [26, 29, 30]. (B) Spin structure. The arrows indicate the spin orientations of iron atoms. The smaller balls indicate the second-layer Te atoms. The spin pattern is alternating one zigzag chain (following nearest Fe-Fe bonds) of spin-up sites and one zigzag chain of spin-down sites, the so-called E-type AFM order [9]. The lattice constant $a_{Te} \sim 3.8$ Å along the AFM direction is slightly longer than b_{Te} along the FM direction [23]. (C) Topography at 77 K (3.3V, 0.03nA, 200nm×200nm denote the bias voltage, tunneling current, and scanning size, respectively) shows the atomically flat surface with broad terraces. The step height is 0.63 nm. The inset shows the Te square lattice (−2.6mV, 0.05nA, 9nm×9nm) without any trace of excess Fe atoms. (D) Topography at 4.2 K (1.5mV, 0.08nA, 15nm×15nm). The inset is the Fourier transformation: the bright spots at $\pm\mathbf{q}_a = (\pm\frac{2\pi}{a_{Te}}, 0)$ and $\pm\mathbf{q}_b = (0, \pm\frac{2\pi}{b_{Te}})$ in the reciprocal space yield $a_{Te}/b_{Te} = 1.02$; the superlattice peaks at $\pm\mathbf{q}_a/2$ reveal a new nematic order with the period of $2a_{Te}$.

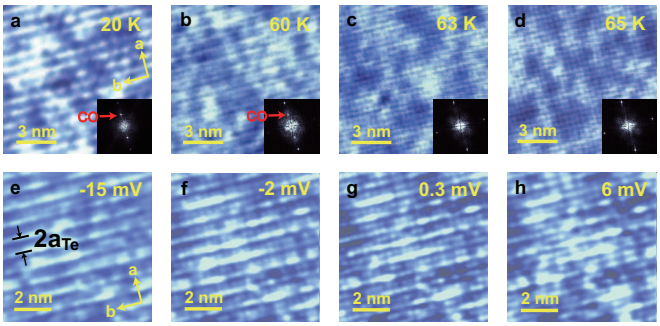

FIG. 2. **Temperature and energy dependences of the CO in FeTe.** (A-D) Temperature dependence of the STM topography (−5mV, 0.02nA, 10nm×10nm). The insets are the corresponding Fourier transformation: The CO bright spot completely disappears above 65 K. (E-H) Bias voltage dependence (0.02nA, 8nm×8nm). The temperature is 4.2 K.

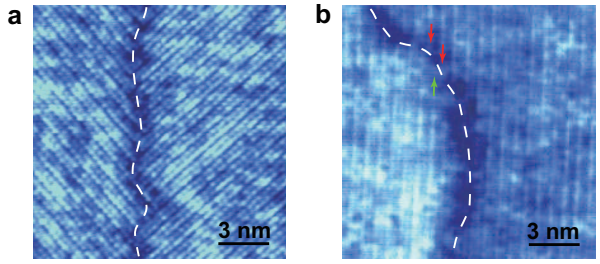

FIG. 3. **Domain boundaries.** (A) Twin boundary (0.2mV, 0.03nA, 15nm×15nm). The direction of stripes rotate by 90°. (B) Anti-phase boundary (−5mV, 0.03nA, 15nm×15nm). Half period is shifted (indicated by the arrows) across the boundary. Dash lines in both images highlight the boundaries.

the charge difference between the spin-up and spin-down Fe sites, especially since the charge fluctuations on the Fe cations and the highly polarizable anions are strongly coupled [19]. This means a novel E-type CO in the Fe plane (see Fig. 4g for a simpler illustration).

The stripe structure of FeTe implies two types of domain boundaries: orthorhombic twin boundary and anti-phase boundary. Both of them have been observed and are shown in Fig. 3. The continuity of the charge stripes ends at the domain boundaries (marked by the dash lines). The stripes either rotate by 90° (Fig. 3A) or shift by $a_{\rm Te}$ (Fig. 3B) upon crossing the boundary while the (1×1)-Te lattice in the topmost layer remains uninterrupted. This rules out the effects of possible defects as the cause of the electronic nematicity (the spontaneous rotational symmetry breaking of the underlying lattice) presented above and further elaborated below.

It is unusual that the CO and the SO have the same periodicity, the $2a_{\rm Te}$ modulation. Usually, the periodicity of charge-density wave (CDW) is half of that of spin-density wave (SDW) [40]. To get insight into the origin of the unique CO in stoichiometric FeTe, we used the STS measurement to reveal a highly anisotropic band dispersion of electronic states. The STS detects the differential tunneling conductance dI/dV, which gives a measure of the local density of states (LDOS) of electrons at energy eV (see Supplementary Note 3 [31] for details). The resultant dI/dV maps at various bias voltages are shown in Figs. 4a-e. The autocorrelation analysis (see the insets of Figs. 4a-e [31]) reveals a wave vector exclusively along the b axis, the FM direction. A parabolic dispersion (Fig. 4f) is obtained by plotting the wave vector versus energy. The dispersion is highly anisotropic and only observed in the FM direction. The parent compound of iron-pnictide superconductor $Ca(Fe_{1-x}Co_x)_2As_2$ also exhibits similar property [33]. However, the present results for FeTe are nontrivial because of their different electron transport behaviours. In FeTe, the electric conductivity along the FM direction is larger than that along the AFM direction [34], while the opposite is observed for iron pnictides [13, 34, 35]. The consistency between the anisotropy in band dispersion and electric conductivity in FeTe unambiguously indicates that the itinerant electrons hop much more easily along the FM direction than along the AFM direction, as previously predicted [9].

Theoretical Analysis.—The vanishing hopping along the AFM direction implies that the charge imbalance between the spin-up and spin-down zigzag chains can occur even for small inter-atomic Coulomb repulsion $\sum_{ij} V_{ij} n_i n_j$, where n_i is the electron number operator on the ith Fe site (see Fig. 4g). Clearly, the $V_{ij} n_i n_j$ term wants to polarize the charge, since the energy minimum of this term is at $n_i = 0$ or $n_j = 0$. Actually, in correlated metals with large resistivity (of the order of mΩ cm), V_{ij} is poorly screened and could be substantially large [22, 36, 37].

To explicitly see how V_{ij} drives the E-type CO in undoped FeTe, we adopt $V_{ij} = 1/\epsilon|\mathbf{r}_i - \mathbf{r}_j|$, where ϵ is the dielectric constant of the material and $\mathbf{r}_i$ the lattice coordinate of the ith Fe site. Let $\tilde{S}_i^z = n_i - \langle n_i\rangle$, where $\langle n_i\rangle$ is the averaged filling of the itinerant electrons per Fe site. Then, the problem is mapped to a classical spin model $\sum_{ij} V_{ij}\tilde{S}_i^z\tilde{S}_j^z$ plus a constant. Retaining V_{ij} up to the third neighbors, namely V_1, V_2, and V_3 (Fig. 4g), and renaming them J_1, J_2, and J_3, respectively, we arrive at the J_1-J_2-J_3 spin model, which is known to yield the E-type AFM spin order when $J_2 > J_1/2$ and $J_3 > J_2/2$ [38]. This criterion is satisfied here by $V_1 : V_2 : V_3 = 2 : \sqrt{2} : 1$ according to the relationship of $|\mathbf{r}_i - \mathbf{r}_j|$ in the Fe square lattice. Hence, the V_{ij} terms alone yield the E-type pattern of CO in its limit of $n_i = 2\langle n_i\rangle$ on the "spin"-up sites and $n_i = 0$ on the "spin"-down sites. This extreme CO will be certainly weakened by the kinetic energy. However, the CO survives via a mechanism similar in spirit to Stoner's itinerant-electron ferromangetism [39] due to the energy gain of $\sim V_3(\langle n_{\rm spin-up-site}\rangle - \langle n_{\rm spin-down-site}\rangle)^2$, as illustrated in Fig. 4h and explicitly demonstrated in a spin-fermion model [9–13] (Supplementary Figure S7 [31]): small V_3 is adequate and necessary to stabilize the CO for realistic $U \sim 2.4$ eV and $J_{\rm H} \sim 0.8$ eV [5]. We stress that the V_{ij} driven Stoner-type mechanism of CO should hold for any model that can account for both the metallic E-type AFM SO and the observed highly anisotropic band dispersion.

The above analysis also provides insight into the question as to why the previous literature [26–29] on $Fe_{1+x}Te$ ($x > 0.07$) showed the CO with the $a_{\rm Te}$ periodicity (see Supplementary Figure S6(b) [31]), half of what we observed. The experimental fact that the amount of excess Fe atoms positively correlates with the degree of electron localization [23, 24] implies that local interactions are enhanced over longer-range ones in the previous materials. This makes V_{ij}'s less important than U. Then, the a_{Te} modulation can appear following the well-known relationship between the characteristic wave vectors of CDW and SDW, $q_{\rm CDW} = 2q_{\rm SDW}$ [29]. Indeed, in re-

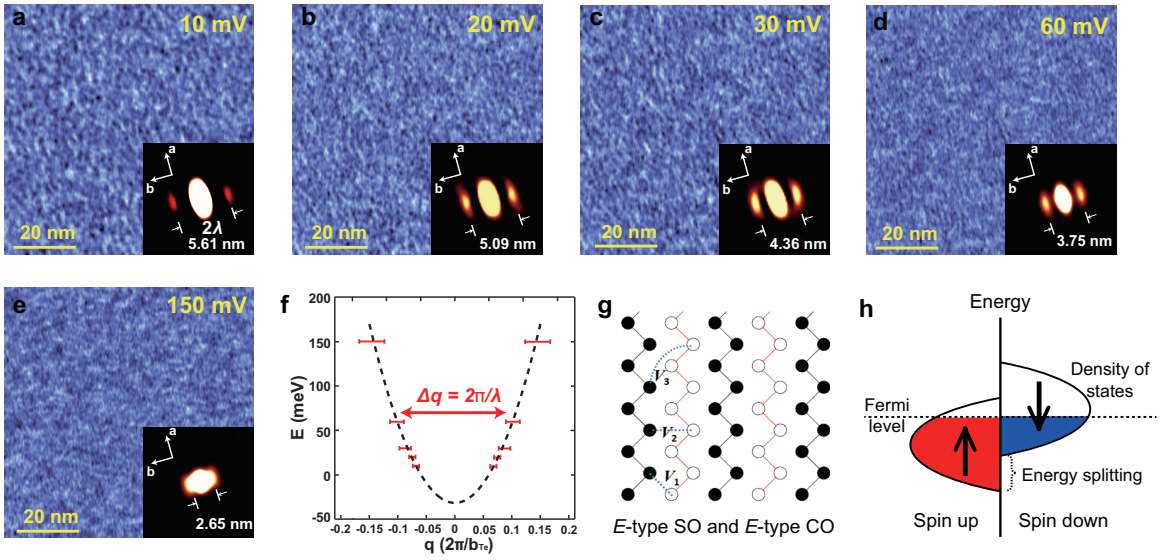

FIG. 4. **Highly anisotropic dispersion of electronic states.** (a-e) dI/dV maps at various bias voltages ($10-150$meV, 0.1nA, 80nm×80nm). The insets are the corresponding 2D auto-correlation images, where half the distance between the two off-center bright spots gives the electronic scattering wavelength λ along the FM direction (see Methods). (f) Dispersion of the itinerant electrons along the FM direction, where $\Delta q = 2\pi/\lambda$. Note that the dispersion along the AFM direction was not detected in (a-e). (g) Schematics of the E-type SO and CO in the Fe sublattice. Solid and open circles stand for charge-rich and charge-poor Fe sites, respectively, while black and red solid lines highlight spin-up and spin-down zigzag chains, respectively. Dotted lines are the guide to the eyes for intersite Coulomb interactions V_1, V_2, and V_3. (h) A schematic band structure for the Stoner ferromagnetism [39], where the energy splitting between states with different spins is $U(\langle n_\uparrow\rangle - \langle n_\downarrow\rangle)$ in the Hubbard model. Now replace the spin-up and spin-down states on the same site (they do not hybridize) in the Hubbard model by the spin-up and spin-down sites in the E-type AFM SO (their hybridization is negligible due to little dispersion along the AFM direction), respectively, and U by V_{ij}. The resultant Stoner "FM" order means the E-type CO with the energy splitting $\sim 4V_3(\langle n_{\rm spin-up-site}\rangle - \langle n_{\rm spin-down-site}\rangle)$.

cent Hartree-Fock calculations of the multiorbital Hubbard model without V_{ij}s, the $a_{\rm Te}$ modulation was found in the considerably large U and J_H region [40]. It can also appear in the spin-fermion model (Supplementary Figure S8 [31]) for $U = 4$ eV and $J_H = 0.8$ eV without V_{ij}'s and for $U = 2.4$ eV, $J_H = 0.8$ eV, $V_1 = 0.15$ eV without V_2 and V_3. With further increase of U, the undoped system will become a robust Mott insulator without CO, whose experimental manifestations are the E-type AFM spin ordered RMnO$_3$ and La$_2$O$_2$Fe$_2$OSe$_2$ [41, 42].

Conclusion.—In many ways, the E-type CO in stoichiometric FeTe is unique: CO in a parent undoped (no apparent mixed-valence) magnetic metal is already rare, in contrast with many other well-known systems with CO such as doped cuprates, doped manganites, intrinsically mixed-valent magnetite, nonmagnetic transition-metal dichalcogenides, insulating LaNiO$_3$, etc. Furthermore, its periodicity is the same as, rather than usually half of, that of AFM SO. These peculiar features provide unambiguously evidence that additional interactions to U and J_H are needed to understand the intermediate regime of $J_{\rm H}$ versus U in general and FeSC in particular. Our further experimental finding of electronic band dispersion only along the FM direction not only confirms a theoretical prediciton [9] but also more importantly implies that the intersite interactions V_{ij} are the most natural candidate for the required additional interactions. We therefore anticipate V_{ij} and charge fluctuations [18, 19], so far much neglected, to be essential to the understanding of FeSC as well as systems in the intermediate regime of $J_{\rm H}$ versus U in general.

This work was supported by National Natural Science Foundation and Ministry of Science and Technology of China and by the U.S. Department of Energy (DOE), Office of Basic Energy Science, under Contract No. DE-AC02-98CH10886.

* wyin@bnl.gov
† xc@mail.tsinghua.edu.cn

[1] E. Dagotto, Science **309**, 257-262 (2005).
[2] A. Georges, L. de Medici, and J. Mravlje, Annu. Rev. Condens. Matter Phys. **4**, 137178 (2013).
[3] I. I. Mazin *et al.*, Phys. Rev. Lett. **98**, 176406 (2007).
[4] M. M. Qazilbash, J. J. Hamlin, R. E. Baumbach, L. Zhang, D. J. Singh, M. B. Maple, and D. N. Basov, Nat. Phys. **5**, 647-650 (2009).
[5] W. L. Yang *et al.*, Phys. Rev. B **80**, 014508 (2009).
[6] Q. Si and E. Abrahams, Phys. Rev. Lett. **101**, 076401 (2008).

[7] L. de' Medici, G. Giovannetti, and M. Capone, Phys. Rev. Lett. **112**, 177001 (2014).

[8] Z. P. Yin, K. Haule, and G. Kotliar, Nat. Mater. **10**, 932-935 (2011).

[9] W.-G. Yin, C.-C. Lee, and W. Ku, Phys. Rev. Lett. **105**, 107004 (2010).

[10] W.-G. Yin, C.-H. Lin, and W. Ku, Phys. Rev. B **86**, 081106(R) (2012).

[11] S.-P. Kou, T. Li, and Z. Y. Weng, Europhys. Lett. **88**, 17010 (2009).

[12] W. Lv, F. Krüger, and P. Phillips, Phys. Rev. B **82**, 045125 (2010).

[13] S. Liang, G. Alvarez, C. Şen, A. Moreo, and E. Dagotto, Phys. Rev. Lett. **109**, 047001 (2012).

[14] F. Krüger, S. Kumar, J. Zaanen, and J. van den Brink, Phys. Rev. B **79**, 054504 (2009).

[15] C.-C. Lee, W.-G. Yin, and W. Ku, Phys. Rev. Lett. **103**, 267001 (2009).

[16] S. Kasahara, H. J. Shi, K. Hashimoto, S. Tonegawa, Y. Mizukami, T. Shibauchi, K. Sugimoto, T. Fukuda, T. Terashima, A. H. Nevidomskyy, and Y. Matsuda, Nature **486**, 382-385 (2012).

[17] S-H. Baek, D. V. Efremov, J. M. Ok, J. S. Kim, J. van den Brink, and B. & Büchner, Nat. Mater. **14**, 210-214 (2014).

[18] S. Zhou, G. G. Kotliar, and Z. Wang, Phys. Rev. B **84**, 140505(R) (2011).

[19] C. Ma, L. Wu, W.-G. Yin, H. Yang, H. Shi, Z. Wang, J. Li, C. C. Homes, and Y. Zhu, Phys. Rev. Lett. **112**, 077001 (2014).

[20] G. A. Sawatzky, I. S. Elfimov, J. van den Brink, and J. Zaanen, Europhys. Lett. **86**, 17006 (2009).

[21] M. Coey, Nature **430**, 155-157 (2004).

[22] D. Volja, W.-G. Yin, and W. Ku, Europhys. Lett. **89**, 27008 (2010).

[23] W. Bao *et al.*, Phys. Rev. Lett. **102**, 247001 (2009).

[24] T. J. Liu, X. Ke, B. Qian, J. Hu, D. Fobes, E. K. Vehstedt, H. Pham, J. H. Yang, M. H. Fang, Phys. Rev. B **80**, 174509 (2009).

[25] U. R. Singh, R. Aluru, Y. Liu, C. Lin, and P. Wahl, Phys. Rev. B **91**, 161111(R) (2015).

[26] T. Machida, K. Kogure, T. Kato, H. Nakamura, H. Takeya, T. Mochiku, S. Ooi, Y. Mizuguchi, Y. Takano, K. Hirata, and H. Sakata, J. Phys. Soc. Jpn. **81**, 074714 (2012).

[27] Y. Kawashima, K. Ichimura, J. Ishioka, T. Kurosawa, M. Oda, K. Yamaya, and S. Tanda, Solid State Communications **167**, 1013 (2013).

[28] T. Machida, K. Kogure, T. Kato, H. Nakamura, H. Takeya, T. Mochiku, S. Ooi, Y. Mizuguchi, Y. Takano, K. Hirata, and H. Sakata, Phys. Rev. B **87**, 214508 (2013).

[29] M. Enayat, Z. Sun, U. R. Singh, R. Aluru, S. Schmaus, A. Yaresko, Y. Liu, C. Lin, V. Tsurkan, A. Loid, J. Deisenhofer, and P. Wahl, Science **345**, 653-656 (2014).

[30] A. Sugimoto, T. Ekino, and A. M. Gabovich, Phys. Rev. B **90**, 224503 (2014).

[31] See Supplemental Material at http://link.aps.org/supplemental/10.1103/PhysRevLett. for technical details.

[32] I. A. Zaliznyak *et al.*, Phys. Rev. Lett. **107**, 216403 (2011).

[33] T.-M. Chuang *et al.*, Science **327**, 181-184 (2010).

[34] J. Jiang *et al.*, Phys. Rev. B **88**, 115130 (2013).

[35] J.-H. Chu *et al.*, Science **329**, 824-826 (2010).

[36] V. J. Emery and S. A. Kivelson, Physica C **263**, 44 (1996).

[37] M. J. Lawler, K. Fujita, J. Lee, A. R. Schmidt, Y. Kohsaka, C. K. Kim, H. Eisaki, S. Uchida, J. C. Davis, J. P. Sethna, and E. -A. Kim, Nature **466**, 347-351 (2010).

[38] F. J. Ma, W. Ji, J. P. Hu, Z.-Y. Lu, and T. Xiang, Phys. Rev. Lett. **102**, 177003 (2009).

[39] E. C. Stoner and P. Roy. Soc. Lond. A **165**, 372-414 (1938).

[40] M. J. Calderón, G. León, B. Valenzuela, and R. Bascones, Phys. Rev. B **86**, 104514 (2012).

[41] T. Hotta *et al.*, Phys. Rev. Lett. **90**, 247203 (2003).

[42] D. G. Free and J. S. O. Evans, Phys. Rev. B **81**, 214433 (2010).